Controlling the magnetic and electric responses of dielectric nanoparticles via near-field coupling

Andrei Kiselev [*] and Olivier J. F. Martin [†]
Nanophotonics and Metrology Laboratory, Department of Microengineering,
École Polytechnique Fédérale de Lausanne, Route Cantonale, 1015 Lausanne, Switzerland

(Received 3 June 2022; revised 9 October 2022; accepted 10 November 2022; published 23 November 2022)

Among the two materials families used in nanophotonics, the fundamental mode for metal nanostructures is electric, while that for dielectric nanostructures is magnetic. Consequently, the optical properties of hybrid dimers that incorporate both materials have prompted significant research. Here, we study the optical response of such hybrid dimers with the coupled electric and magnetic dipoles method, and demonstrate how their electromagnetic interactions can be used to modulate the electric and magnetic responses. The conditions for the complete suppression of the magnetic dipole in the visible range for high refractive index dielectric nanoparticles are described. The electric and magnetic responses can be enhanced or reduced by positioning the dielectric particle in the nodes of the standing wave formed by the metallic particle. This controlled near-field interaction provides a handle on the near- and far-field responses of the system, with possible applications such as sensing and optical switches.

DOI: 10.1103/PhysRevB.106.205413

I. INTRODUCTION

The first-order multipoles: The electric and magnetic dipoles show distinct properties that require to consider them separately [1]. Metallic nanoparticles usually possess a strong electric dipolar response, which allows them to generate strong electric fields with a $1/r^3$ near-field dependence [2,3]. On the other hand, the magnetic near-field enhancement has only a $1/r^2$ leading term and therefore is much smaller compared to the electric component. On the quest to generate large magnetic fields in the vicinity of nanoparticles, dielectric materials with high refractive index have recently emerged [4,5]. Their prime resonance is the magnetic dipole, which generates a strong magnetic near field with a $1/r^3$ dependence and only a $1/r^2$ dependence for the electric field. The ability to have a strong magnetic field enhancement can affect the radiation properties of magnetic dipole emitters, such as lanthanide ions (Er^{3+}, Ho^{3+}, and Dy^{3+}) [6–8]. Also, the magnetic dipoles feel a repelling force from a surface, whereas the electric dipoles are usually attracted to their image [9,10]. Altogether, the electric and magnetic resonances can lead to Kerker-type effects that significantly affect the radiation directivity [11–14].

The ability to selectively engineer electric or magnetic responses for an object is an important challenge that has been addressed by several authors. It was, for example, shown that by using specific beam symmetries, it is possible to suppress electric or magnetic scattering components of the object [15,16]. The geometrical modification of the object also allows to control the multipolar response [11,17–20]. The utilization of dielectric and metallic shells can suppress selected multipoles [10,21–23]. Another approach to engineer the scattering is the near-field coupling. This approach is interesting since it allows to manipulate the coupling strength by controllably positioning interacting objects to obtain the required response. This topic has attracted particular interest.

Engineering light scattering from a collection of particles can find many applications in optics. Already a pair of metallic nanoparticles can engineer the spectral response of the system [24–26]. When additional particles are added, new degrees of freedom emerge that can be used to control the spectrum [27–31], the radiation properties [32,33], or some other optical properties like chirality [34]; extremely narrow resonances can be observed in longer particle chains [35–38]. The effects offered by metallic nanoparticles can be used to enhance the efficiency of plasmonic sensors [39,40], especially for surface-enhanced Raman spectroscopy [41] and fluorescence-based biosensing [42]; plasmonic nanoclusters help pushing the limits for interparticle distance measurements [43,44], play a role in heat-assisted magnetic recording [45] and optical trapping [46–48].

For a cluster of nanoparticles, both the multipoles excited in the individual particles and their mutual interactions play a role. For example, it was shown that the coupling between two electric dipoles broadens the overall scattering response [49]. Two magnetic dipoles, on the contrary, can make the spectral line narrower. The electromagnetic coupling in clusters enables efficient magnetic dipole generation [19,50–52], while the generation of electric and magnetic hot spots in clusters was discussed [2,7,53–58]. It also was shown that the magnetic dipole mode of an isolated particle can couple to the mode of a dielectric oligomer to produce very distinct Fano feature with strong suppression of the total scattering cross section [50,59] or reflection [49]. Magnetic Fano resonances can be tuned through laser-induced reshaping [60]. Coupling between nanoobjects can significantly alter the far-field scattering directivity [11,52,54,61–66]. The eigenmode

[*] andrei.kiselev@epfl.ch
[†] olivier.martin@epfl.ch

analysis was shown to be efficient in describing scattering from coupled particles [22,67]. An antiferromagnetic field distribution was achieved in a metamaterial composed of a dielectric sphere and a split ring metal resonator [68]. Resonant electromagnetic coupling enabled the generation of a strong pulling force in metal-dielectric dimers [69].

In this paper, similarly to previously shown achievements in enhancing the magnetic response with structured light [15,16] or by using the near-field coupling as discussed in the review [55], we manage to completely suppress the magnetic response in a dielectric structure. We exploit a known phenomenon where a standing wave can help diminishing or enhancing the individual multipolar components of an object [70]. To achieve that, a metallic nanosphere is used as a strong backscatterer, which, along with the incident wave, produces a standing wave. By placing an additional dielectric nano-object in the vicinity of this metallic nanosphere, the magnetic response of the dielectric nanoparticle is completely suppressed at a selected wavelength. In Sec. II the multipolar scattering responses from individual subwavelength metal and dielectric spheres are discussed. Then, in Sec. III, the response of a metal-dielectric dimer is presented. For short interparticle distances, complete suppression of the magnetic dipole is observed in the dielectric. The near- and far-fields manifestations of this effect are discussed in Sec. III. The explanation of the observed effect is given in Sec. IV by considering the formation of a standing wave between the incident field and the light scattered from the metal particle. Similar studies were performed for absorption modulations in standing waves [70–73]. Finally, the effect of magnetic dipole enhancement, accompanied by the electric dipole reduction in dielectric is investigated in Sec. V. The SI unit system is used throughout and the time dependence $\exp(-i\omega t)$ is assumed.

II. SCATTERING FROM INDIVIDUAL METAL AND DIELECTRIC NANOPARTICLES

Mie theory provides analytical solutions for the scattering from spherical objects [74]. Within this framework, the multipolar expansion serves as the conventional basis for the solution of the electromagnetic field. The first lowest-order terms — electric dipolar (ED) and magnetic dipolar (MD) — in this expansion are usually sufficient to describe the scattering within the visible range for metallic or dielectric objects having sizes smaller than ≈80 nm [54]. In Fig. 1 we plot the total scattering cross section (SCS) along with the dipolar and electric quadrupolar contributions (EQ) to the scattering for a TiO_2 sphere with radius $R_1 = 75$ nm, Figs. 1(a) and 1(b), and for an Ag sphere, Figs. 1(c) and 1(d), with radius $R_2 = 50$ nm. The refractive index for TiO_2 is approximated as constant $n = 2.6$ [75], the data from Johnson and Christy are taken for Ag [76] and the refractive index of the background medium is considered to be equal to 1 for all the simulations performed in this article. Figure 1 indicates that the maximum SCS magnitude for each individual sphere is of the same order; the response of the dielectric sphere includes both an electric and a magnetic dipoles, while the metallic particle has only an electric dipole resonance [4]. This is because the refractive index of TiO_2 is $n \approx 2.6$, whereas for silver $n \approx 0.05$. The excitation of the magnetic dipole can be achieved only in high

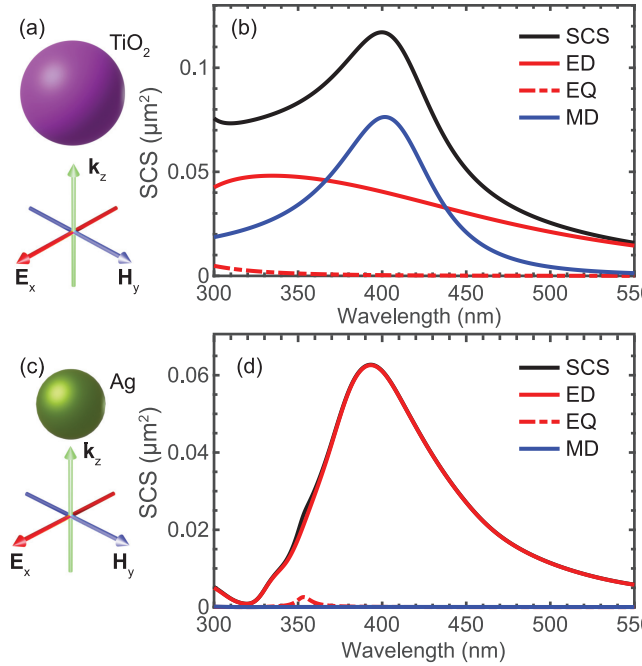

FIG. 1. (a) Sketch of the TiO_2 sphere with radius $R_1 = 75$ nm illuminated with a plane wave. (b) Scattering cross section and its electric dipolar (ED), magnetic dipolar (MD), and electric quadrupolar (EQ) contributions. (c) Sketch of the Ag sphere with radius $R_2 = 50$ nm illuminated with a plane wave and (d) its corresponding scattering cross section.

index dielectric where the effective wavelength λ/n is small [4], as will be discussed in details in Sec. IV. Higher-order multipoles are negligible for those nanostructures.

III. SCATTERING RESPONSE FROM A HYBRID DIMER

Let us now discuss the scattering properties of a dimer composed of the TiO_2 and Ag nanoparticles considered in Sec. II. The gap between the two particles is $g = 10$ nm. The dimer is illuminated with a plane wave propagating along the symmetry axis of the system, Fig. 2(a). We refer the reader to Ref. [64], where the coupled electric and magnetic dipole method (CEMD) equations are written. For the TiO_2 nanoparticle within the dimer we introduce the magnitudes of the electric (p_{TiO_2}) and magnetic (m_{TiO_2}) dipoles and for the Ag nanoparticle within the dimer we introduce similarly (p_{Ag}) and (m_{Ag}). After solving the CEMD equations [64], the total scattering cross section can be found as $C_{scs} = C_{ext} - C_{abs}$, where C_{ext} and C_{abs} are the extinction and absorption scattering cross sections found in the dipolar approximation as [77–79]

$$C_{ext} = \frac{k}{\varepsilon_0 |E_0|^2} \sum_{j=1}^{2} \mathrm{Im}(\mathbf{E}^*_{inc,j}\mathbf{p}_j + \mu_0 \mathbf{H}^*_{inc,j}\mathbf{m}_j), \tag{1}$$

$$C_{abs} = \frac{k}{\varepsilon_0 |E_0|^2} \sum_{j=1}^{2} \mathrm{Im}\left[\left(\frac{\mathbf{p}^*_j \mathbf{p}_j}{\alpha_{e,j}} - \frac{2}{3}k^3 |\mathbf{p}_j|^2\right) + \mu_0 \left(\frac{\mathbf{m}^*_j \mathbf{m}_j}{\alpha_{m,j}} - \frac{2}{3}k^3 |\mathbf{m}_j|^2\right)\right]. \tag{2}$$

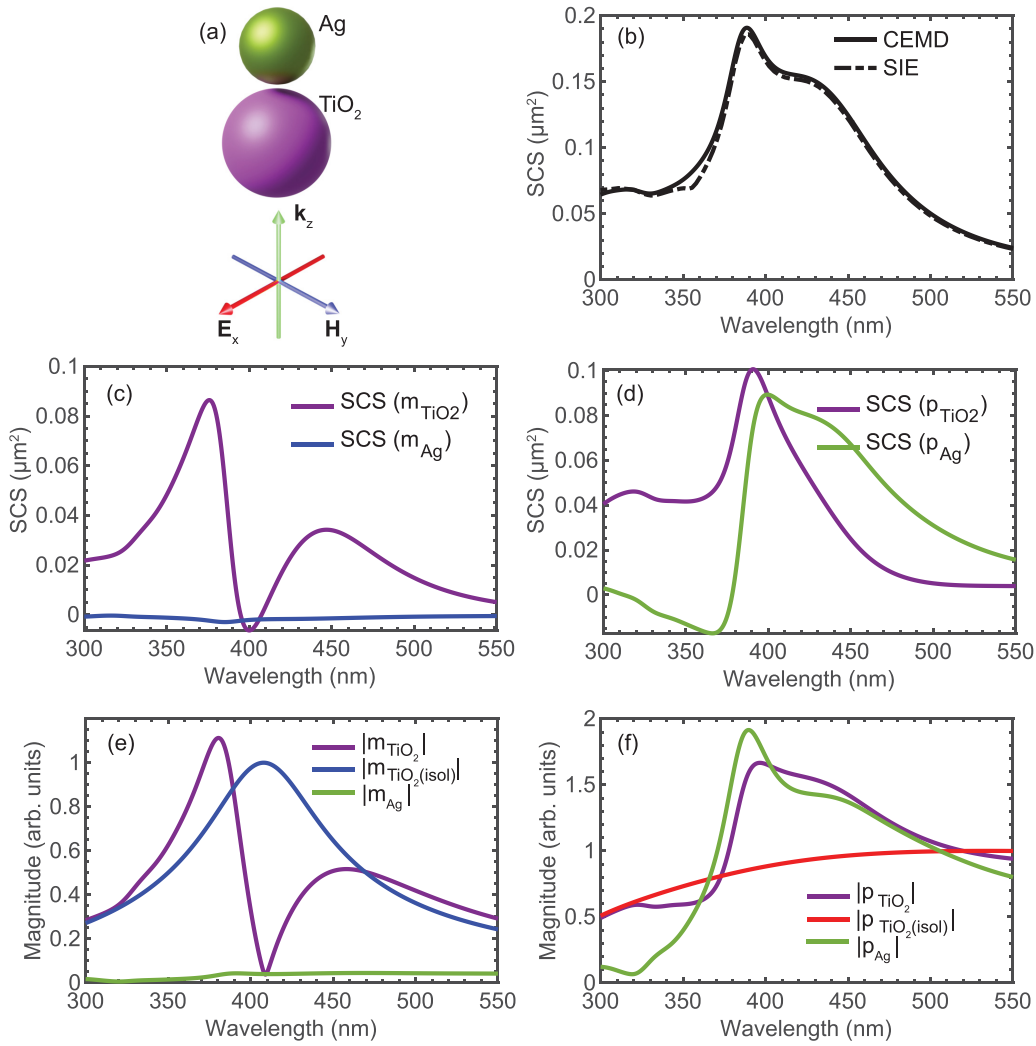

FIG. 2. (a) Sketch of the hybrid dimer containing the Ag sphere with radius $R_2 = 50$ nm placed on top of the TiO_2 sphere with radius $R_1 = 75$ nm and separated by the interparticle distance $g = 10$ nm. The system is illuminated with a plane wave propagating along its symmetry axis. (b) Comparison of the scattering cross sections obtained with the CEMD and SIE methods. (c)–(f) Scattering cross-section contributions and magnitudes of the magnetic and electric dipoles excited in the TiO_2 and Ag nanoprticles within the hybrid system. In panels (e) and (f) the magnitudes of the dipoles excited in the isolated 75 nm TiO_2 sphere are provided for comparison. The magnitude of the dipoles is normalized to the maximum value obtained for the isolated TiO_2 nanoparticle.

Here, E_0 is the amplitude of the incident electric field, $k = 2\pi/\lambda$, ε_0, μ_0, and c are, respectively, the wave number, permittivity, and permeability of a vacuum and the speed of light in a vacuum, the electric and magnetic dipoles are found as $\mathbf{p}_j = \varepsilon_0 \alpha_{e,j} \mathbf{E}_j$, $\mathbf{m}_j = \alpha_{m,j} \mathbf{H}_j$ and the polarizabilities are $\alpha_{e,j} = i6\pi a_{1,j}/k^3$ and $\alpha_{m,j} = i6\pi b_{1,j}/k^3$ defined via the Mie coefficients $a_{1,j}$ and $b_{1,j}$ for each particle with index j [74]; the sign * indicates the complex conjugate. Assuming that the two particles are placed at $(0, 0, \pm d/2)$, $d = R_1 + R_2 + g$, within the framework of the CEMD theory, we verify the accuracy of the CEMD method, by plotting in Fig. 2(b) the total scattering cross section found with the CEMD method and compare it with the full wave simulations based on the surface integral equation (SIE) method [80,81]. As can be seen, the results show very good agreement for the entire wavelength range, except for the region close to 360 nm. This difference can be explained by the fact that the isolated Ag nanoparticle has a quadrupolar resonance at 355 nm that is not included in the CEMD model, Fig. 1(d).

The scattering cross-section contributions from individual multipoles obtained by subtracting Eq. (2) from Eq. (1) are presented in Figs. 2(c) and 2(d); the normalized magnitudes of the magnetic and electric multipoles for a dimer are presented in Figs. 2(e) and 2(f). We also plot in Figs. 2(e) and 2(f) the magnitudes of the electric ($p_{TiO_2(isol)}$) and magnetic ($m_{TiO_2(isol)}$) dipoles for the isolated TiO_2 particle considered in Sec. II. As can be seen from Figs. 2(c) and 2(e), the magnitude of the TiO_2 magnetic dipole in the dimer is almost completely suppressed at $\lambda = 409$ nm. With the weak magnetic response in Ag the overall magnetic response of the system becomes negligible, Figs. 2(c) and 2(e). This affects quite substantially the near- and far-fields of the dimer.

In Fig. 3, the magnetic field distribution is presented for the dimer for the cases when the magnetic response in TiO_2 is strong (at 380 nm) and weak (at 409 nm), see Fig. 2(c).

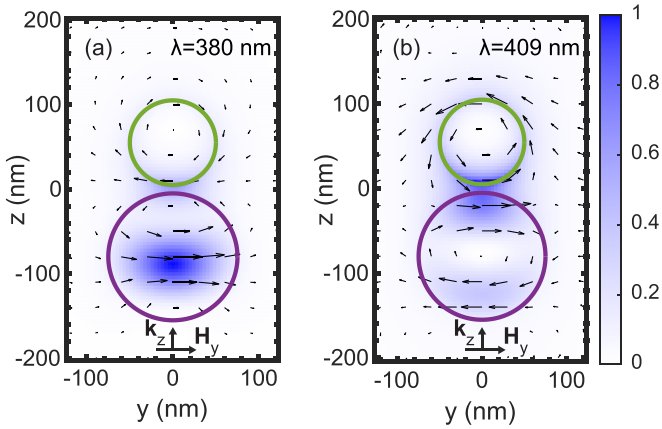

FIG. 3. Colormap of the normalized magnetic scattered field intensity computed for (a) the maximum and (b) the minimum of the magnetic responses in TiO_2, see Fig. 2(c). The arrows represent the real part of the scattered magnetic field.

The near-field graph is plotted in the yz-plane for $x = 0$ nm using the SIE. It can be clearly noticed that the strong magnetic response at $\lambda = 380$ nm provides the magnetic dipolar near-field distribution in TiO_2. It can also be seen that the maximum of the magnetic field is reached at the center of TiO_2. The vortex-like distribution of the magnetic field in Ag indicates the presence of the strong electric dipole response [82]. For the dimer at $\lambda = 409$ nm, the magnetic dipole response in TiO_2 is suppressed and only two vortices attributed to strong electric dipoles in both nanoparticles can be seen. It is interesting to note that the maximum of the magnetic field is now shifted towards the space between the two particles.

The cancellation of the magnetic dipole in both nanoparticles has important implications for the far field. Indeed, let us consider the intensity registered at a detector placed along the x-axis 10 μm away from the dimer, as shown in Fig. 4(a). The intensity spectra (normalized with respect to the incident wave) are shown in Fig. 4(b) for isolated TiO_2 and for the dimer. It is clearly seen that the magnitude of the intensity drops significantly at $\lambda = 409$. This is explained by the fact that the radiation pattern of the magnetic dipole, shown in Fig. 4(a) (blue color), has its maximum within the xz-plane and no radiation along the y-axis. In the same way, the electric dipole excited in the dimer [shown in red color in Fig. 4(a)] produces no radiation along the x-axis. Consequently, the cancellation of the magnetic dipole can be observed with far-field measurements and this configuration can be used as a switch where the "on/off" states are controlled by the interparticle distance. Actually, such a polarization controlled switch was realized in the microwave in Ref. [62], where the intensity control in the lateral direction was performed by illuminating Si-Si dimers with different interparticle distances. The observation of such an effect in the optical range is more challenging, but could be potentially implemented with the modified dark-field setup discussed in Ref. [83].

IV. STANDING WAVE

Let us now discuss the origin of the previously observed magnetic dipole suppression. In Fig. 5(a) we plot the distribution of the normalized electric $w_e/w_{e(inc)} = E(r)E^*(r)/[E_{inc}(r)E_{inc}{}^*(r)]$ and magnetic $w_m/w_{m(inc)} = H(r)H^*(r)/[H_{inc}(r)H_{inc}{}^*(r)]$ energy densities as a function of coordinate for *isolated* Ag sphere having radius 50 nm illuminated with a plane wave propagating from left to right. Here "inc" stands for the fields generated by the incident wave, $E_{inc}(r) = E_0 e^{ikz}$ and $H_{inc}(r) = \varepsilon_0 c E_{inc}(r)$. This graph is plotted in the dipolar approximation where the electric field along the x-axis is defined by

$$E(z) = E_{inc}(r) + \frac{k^2 A(z) p_{Ag(isol)}}{\varepsilon_0} + i\frac{k^2}{\varepsilon_0 c} B(z) m_{Ag(isol)}, \quad (3)$$

and the magnetic field as

$$H(z) = H_{inc}(r) + ick^2 B(z) p_{Ag(isol)} + k^2 A(z) m_{Ag(isol)}. \quad (4)$$

Here, $A(z) = [1 + i/kz - 1/(kz)^2]e^{ikz}/4\pi z$, $B(z) = [i - 1/(kz)]e^{ikz}/4\pi z$. The Ag particle is placed at $z = 0$ nm.

From Fig. 5(a) it becomes clear that the magnitude of the magnetic energy reaches the first node at ≈ -130 nm. Consequently, one would expect that placing another nanoparticle at this position would not cause any magnetic response in it. This can also be understood from the inset presented in Fig. 5(a) where a nanoparticle is illuminated first with a single

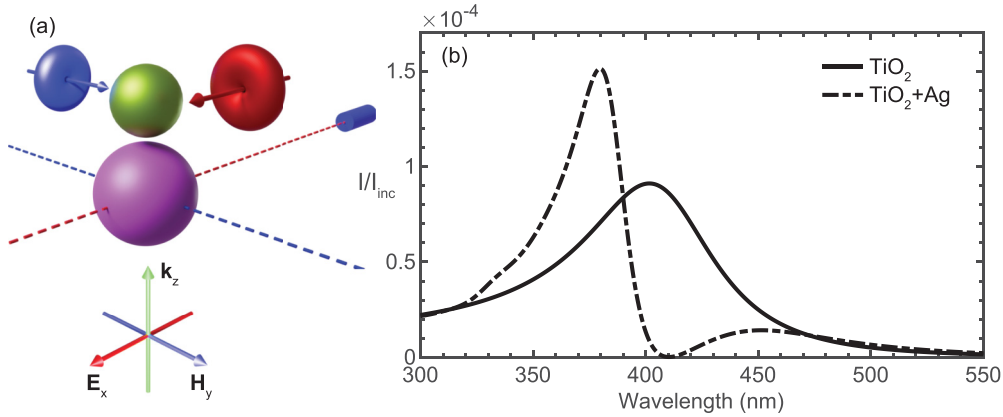

FIG. 4. (a) Sketch of the hybrid system illuminated with a plane wave, together with the radiation patterns of the excited electric (in red) and magnetic (in blue) dipoles. The intensity detector is shown as the blue cylinder. (b) Intensities registered with the detector for isolated TiO_2 and hybrid TiO_2-Ag structures. The intensities are normalized with respect to the intensity of the incident wave.

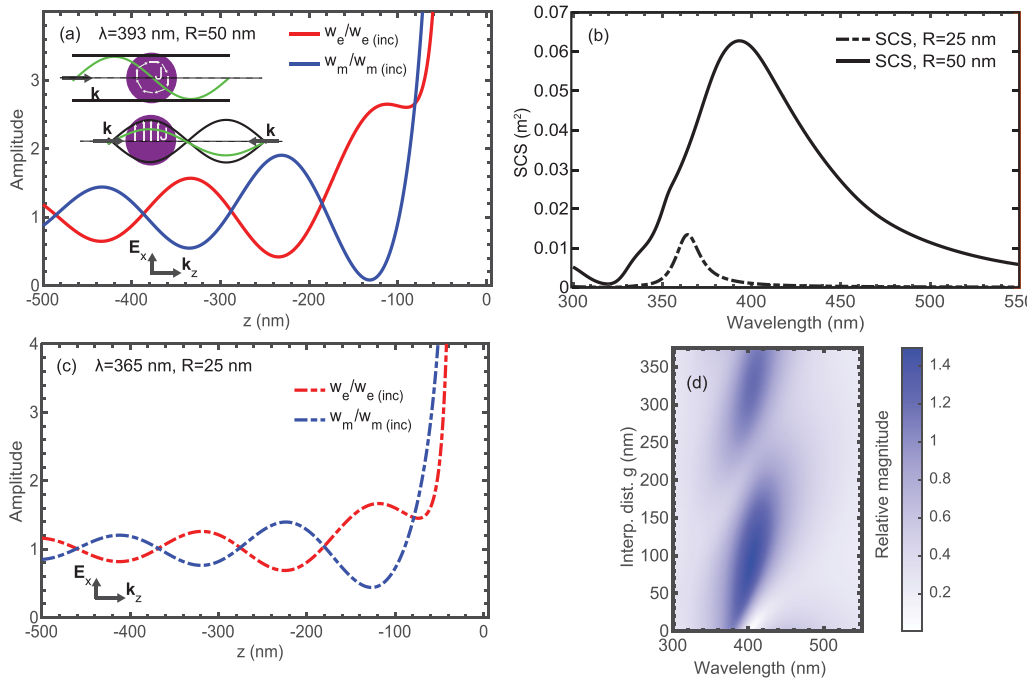

FIG. 5. Distributions of the total electric and magnetic intensities for (a) 50 nm and (c) 25 nm Ag spheres at the corresponding resonance wavelengths. Inset: The envelope of the electric field amplitude is shown as black solid lines. The instantaneous spatial distribution of the incident electric field at an arbitrary instance of time shown is green. White arrows represent the distribution of the induced current inside the particle. (b) Scattering cross sections for Ag spheres with the radii of 25 and 50 nm. (d) Magnitude of the magnetic dipole in TiO_2 for TiO_2-Ag hybrid systems as a function of the interparticle distance g. The magnitude is normalized with respect to the maximum of $|m_{TiO_2(isol)}|$ obtained in Fig. 2(c).

plane wave and the instantaneous electric field distribution is shown with green color. The retardation effect causes the current to flow in opposite directions at both extremities of the nanoparticle (top inset), thus leading to a strong magnetic response. For the standing wave case, when two plane waves illuminate from opposite directions, the magnetic field has the node at the position of the particle whereas the electric field has its maximum. Thus, the particle cannot acquire any circulating current and no magnetic response is observed (bottom inset).

It also turns out that the size of the metallic particle plays a major role in the magnetic suppression effect. In Fig. 5(b) the scattering cross section for Ag particles with 50 nm and 25 nm radii are shown. The maximum of the scattering cross section is approximately six times enhanced and red-shifted for the 50-nm sphere as compared to the 25-nm one. For a 25-nm sphere, the scattered field is much weaker and unable to produce a full standing wave, as can be seen from Fig. 5(c). Consequently, a sufficiently large sphere is required to achieve the effect. We also studied this effect with other plasmonic materials (Al, Cu [84], Au [76], W, Pt [85]). Our results show that only Al has a sufficiently strong scattered field to reach the same effect as Ag at a wavelength close to 400 nm. However, the electric quadrupole has also a significant contribution in this case, which makes the application of the CEMD model inappropriate.

Finally, let us study the influence of the interparticle distance g on the magnitude of the magnetic dipole excited in TiO_2 for the TiO_2-Ag dimer considered previously, Fig. 5(d). As can be seen, the magnetic dipole is reduced only for small interparticle distances below 30 nm, which is consistent with the results obtained in Fig. 5(a).

V. CONTROL OF INDIVIDUAL DIPOLES

In this section we show that the electric dipole can also be controlled in the considered dimer. As stems from Fig. 5(a), the electric and magnetic energy densities exhibit oscillating behaviors as a function of the z-coordinate. Consequently, by placing the dielectric particle at the position where the magnetic energy reaches a local maximum, we can increase the magnetic response from the dielectric particle. Note that this position corresponds to the minimum of the electric energy density, as follows from Fig. 5(a), and the electric dipole response in the dielectric particle will be consequently reduced. This is demonstrated in Fig. 6, where the magnitudes of the electric and magnetic dipoles are plotted as a function of wavelength for the interparticle distance $g = 92$ nm, corresponding to the local maximum of the magnetic energy observed at $z = -230$ nm in Fig. 5(a). As can be seen from Fig. 6 this interparticle distance indeed leads to a reduction of the electric dipole and the enhancement of the magnetic dipole in TiO_2. Hence, the radiative coupling between the electric dipolar and magnetic dipolar modes can enhance the magnetic response in TiO_2.

In the previous discussion the materials and sizes of metallic and dielectric nanoparticles were optimized to achieve the most prominent effect. One could wonder what would have happened if different parameters for the interacting nanoparticles had originally been chosen or the particles were swapped

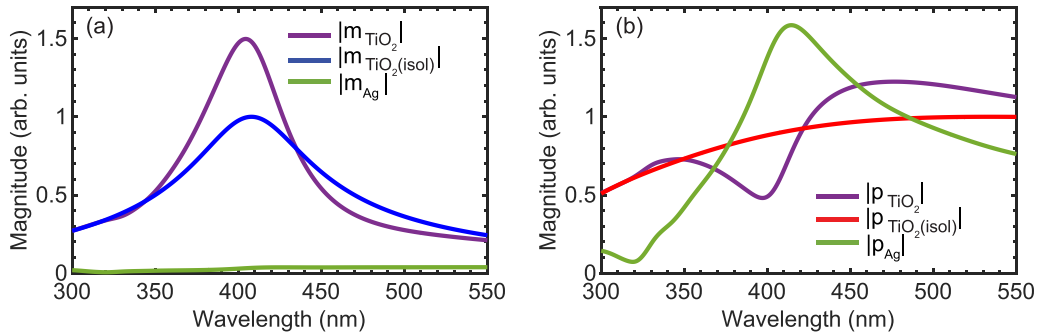

FIG. 6. Magnitudes of the (a) magnetic and (b) electric dipoles excited in TiO_2 and Ag in a hybrid system with the interparticle distance $g = 92$ nm and the magnitudes of the dipoles excited in isolated TiO_2. The normalization of the dipoles is performed with respect to the maximum of the corresponding magnitude in the isolated TiO_2.

in the considered geometry. From the previous analysis we can conclude that the multipole reduction effect must also take place, although less prominently.

VI. CONCLUSION

We showed that the multipolar response of a TiO_2 subwavelength dielectric sphere that is expected to have simultaneously strong electric and magnetic dipole responses in the visible range can be significantly modified by bringing an Ag sphere in a close proximity. In particular, the magnetic response can be either enhanced or completely suppressed. The observed effect is explained by the formation of a standing wave resulting from the interference between the incident field and the light scattered by the Ag sphere. This effect can be used to manipulate both the near- and the far-field distributions.

ACKNOWLEDGMENTS

We gratefully acknowledge funding from the European Research Council (Grant No. ERC-2015-AdG-695206 Nanofactory).

[1] M. Riccardi, A. Kiselev, K. Achouri, and O. J. F. Martin, Multipolar expansions for scattering and optical force calculations beyond the long wavelength approximation, Phys. Rev. B **106**, 115428 (2022).

[2] C. Girard, A. Dereux, O. J. F. Martin, and M. Devel, Importance of confined fields in near-field optical imaging of subwavelength objects, Phys. Rev. B **50**, 14467 (1994).

[3] J. D. Jackson, *Classical Electrodynamics* (John Wiley & Sons, New York, 2007).

[4] A. I. Kuznetsov, A. E. Miroshnichenko, Y. H. Fu, J. Zhang, and B. Luk'Yanchuk, Magnetic light, Sci. Rep. **2**, 492 (2012).

[5] B. Lukyanchuk, L. Vasilyak, V. Y. Pecherkin, S. Vetchinin, V. Fortov, Z. Wang, R. Paniagua-Domínguez, and A. Fedyanin, Colossal magnetic fields in high refractive index materials at microwave frequencies, Sci. Rep. **11**, 23453 (2021).

[6] B. Rolly, B. Bebey, S. Bidault, B. Stout, and N. Bonod, Promoting magnetic dipolar transition in trivalent lanthanide ions with lossless mie resonances, Phys. Rev. B **85**, 245432 (2012).

[7] Z.-J. Yang, Q. Zhao, and J. He, Boosting magnetic field enhancement with radiative couplings of magnetic modes in dielectric nanostructures, Opt. Express **25**, 15927 (2017).

[8] D. G. Baranov, R. S. Savelev, S. V. Li, A. E. Krasnok, and A. Alù, Modifying magnetic dipole spontaneous emission with nanophotonic structures, Laser Photonics Rev. **11**, 1600268 (2017).

[9] P. Gay-Balmaz and O. J. Martin, Validity domain and limitation of non-retarded green's tensor for electromagnetic scattering at surfaces, Opt. Commun. **184**, 37 (2000).

[10] J. J. Kingsley-Smith, M. F. Picardi, and F. J. Rodríguez-Fortuño, Optical magnetic dipole levitation using a plasmonic surface, Nano Lett. **20**, 7094 (2020).

[11] W. Liu and Y. S. Kivshar, Generalized kerker effects in nanophotonics and meta-optics, Opt. Express **26**, 13085 (2018).

[12] H. K. Shamkhi, K. V. Baryshnikova, A. Sayanskiy, P. Kapitanova, P. D. Terekhov, P. Belov, A. Karabchevsky, A. B. Evlyukhin, Y. Kivshar, and A. S. Shalin, Transverse Scattering and Generalized Kerker Effects in All-Dielectric Mie-Resonant Metaoptics, Phys. Rev. Lett. **122**, 193905 (2019).

[13] K. Koshelev and Y. Kivshar, Dielectric resonant metaphotonics, ACS Photonics **8**, 102 (2021).

[14] M. M. Bukharin, V. Y. Pecherkin, A. K. Ospanova, V. B. Il'in, L. M. Vasilyak, A. A. Basharin, and B. Luk'yanchuk, Transverse kerker effect in all-dielectric spheroidal particles, Sci. Rep. **12**, 7997 (2022).

[15] T. Das, P. P. Iyer, R. A. DeCrescent, and J. A. Schuller, Beam engineering for selective and enhanced coupling to multipolar resonances, Phys. Rev. B **92**, 241110(R) (2015).

[16] J. Zeng, M. Darvishzadeh-Varcheie, M. Albooyeh, M. Rajaei, M. Kamandi, M. Veysi, E. O. Potma, F. Capolino, and H. K. Wickramasinghe, Exclusive magnetic excitation enabled by structured light illumination in a nanoscale mie resonator, ACS Nano **12**, 12159 (2018).

[17] N. Liu, L. Fu, S. Kaiser, H. Schweizer, and H. Giessen, Plasmonic building blocks for magnetic molecules in three-dimensional optical metamaterials, Adv. Mater. **20**, 3859 (2008).

[18] F. Shafiei, F. Monticone, K. Q. Le, X.-X. Liu, T. Hartsfield, A. Alù, and X. Li, A subwavelength plasmonic metamolecule exhibiting magnetic-based optical fano resonance, Nat. Nanotechnol. **8**, 95 (2013).

[19] R. Verre, Z. J. Yang, T. Shegai, and M. Käll, Optical magnetism and plasmonic fano resonances in metal–insulator–metal oligomers, Nano Lett. **15**, 1952 (2015).

[20] A. I. Kuznetsov, A. E. Miroshnichenko, M. L. Brongersma, Y. S. Kivshar, and B. Luk'yanchuk, Optically resonant dielectric nanostructures, Science **354**, aag2472 (2016).

[21] T. Feng, Y. Xu, W. Zhang, and A. E. Miroshnichenko, Ideal Magnetic Dipole Scattering, Phys. Rev. Lett. **118**, 173901 (2017).

[22] M. Pascale, G. Miano, and C. Forestiere, Spectral theory of electromagnetic scattering by a coated sphere, J. Opt. Soc. Am. B **34**, 1524 (2017).

[23] C. Forestiere, G. Miano, M. Pascale, and R. Tricarico, Directional scattering cancellation for an electrically large dielectric sphere, Opt. Lett. **44**, 1972 (2019).

[24] R. Ruppin, Optical absorption of two spheres, J. Phys. Soc. Jpn. **58**, 1446 (1989).

[25] H. Fischer and O. J. F. Martin, Engineering the optical response of plasmonic nanoantennas, Opt. Express **16**, 9144 (2008).

[26] J. Zuloaga, E. Prodan, and P. Nordlander, Quantum description of the plasmon resonances of a nanoparticle dimer, Nano Lett. **9**, 887 (2009).

[27] C. Rockstuhl, M. G. Salt, and H. P. Herzig, Analyzing the scattering properties of coupled metallic nanoparticles, J. Opt. Soc. Am. A **21**, 1761 (2004).

[28] M. Hentschel, D. Dregely, R. Vogelgesang, H. Giessen, and N. Liu, Plasmonic oligomers: The role of individual particles in collective behavior, ACS Nano **5**, 2042 (2011).

[29] A. Lovera, B. Gallinet, P. Nordlander, and O. J. Martin, Mechanisms of fano resonances in coupled plasmonic systems, ACS Nano **7**, 4527 (2013).

[30] S. Dutta-Gupta and O. J. F. Martin, Insight into the eigenmodes of plasmonic nanoclusters based on the green's tensor method, J. Opt. Soc. Am. B **32**, 194 (2015).

[31] N. S. King, L. Liu, X. Yang, B. Cerjan, H. O. Everitt, P. Nordlander, and N. J. Halas, Fano resonant aluminum nanoclusters for plasmonic colorimetric sensing, ACS Nano **9**, 10628 (2015).

[32] A. J. Pasquale, B. M. Reinhard, and L. Dal Negro, Engineering photonic–plasmonic coupling in metal nanoparticle necklaces, ACS Nano **5**, 6578 (2011).

[33] P. Albella, M. A. Poyli, M. K. Schmidt, S. A. Maier, F. Moreno, J. J. Sáenz, and J. Aizpurua, Low-loss electric and magnetic field-enhanced spectroscopy with subwavelength silicon dimers, J. Phys. Chem. C **117**, 13573 (2013).

[34] A. Guerrero-Martínez, J. L. Alonso-Gómez, B. Auguié, M. M. Cid, and L. M. Liz-Marzán, From individual to collective chirality in metal nanoparticles, Nano Today **6**, 381 (2011).

[35] L. Zhao, K. L. Kelly, and G. C. Schatz, The extinction spectra of silver nanoparticle arrays: Influence of array structure on plasmon resonance wavelength and width, J. Phys. Chem. B **107**, 7343 (2003).

[36] S. Zou, N. Janel, and G. C. Schatz, Silver nanoparticle array structures that produce remarkably narrow plasmon lineshapes, J. Chem. Phys. **120**, 10871 (2004).

[37] D. Brunazzo, E. Descrovi, and O. J. F. Martin, Narrowband optical interactions in a plasmonic nanoparticle chain coupled to a metallic film, Opt. Lett. **34**, 1405 (2009).

[38] V. G. Kravets, A. V. Kabashin, W. L. Barnes, and A. N. Grigorenko, Plasmonic surface lattice resonances: A review of properties and applications, Chem. Rev. **118**, 5912 (2018).

[39] J. N. Anker, W. P. Hall, O. Lyandres, N. C. Shah, J. Zhao, and R. P. Van Duyne, Biosensing with plasmonic nanosensors, in *Nanoscience and Technology* (World Scientific, Singapore, 2010), pp. 308–319.

[40] A. Minopoli, A. Acunzo, B. Della Ventura, and R. Velotta, Nanostructured surfaces as plasmonic biosensors: A review, Adv. Mater. Interfaces **9**, 2101133 (2022).

[41] A. Kumar, S. Kim, and J.-M. Nam, Plasmonically engineered nanoprobes for biomedical applications, J. Am. Chem. Soc. **138**, 14509 (2016).

[42] M. A. Badshah, N. Y. Koh, A. W. Zia, N. Abbas, Z. Zahra, and M. W. Saleem, Recent developments in plasmonic nanostructures for metal enhanced fluorescence-based biosensing, Nanomaterials **10**, 1749 (2020).

[43] C. Sönnichsen, B. M. Reinhard, J. Liphardt, and A. P. Alivisatos, A molecular ruler based on plasmon coupling of single gold and silver nanoparticles, Nat. Biotechnol. **23**, 741 (2005).

[44] B. Gallinet, T. Siegfried, H. Sigg, P. Nordlander, and O. J. F. Martin, Plasmonic radiance: Probing structure at the Ångström scale with visible light, Nano Lett. **13**, 497 (2013).

[45] M. H. Kryder, E. C. Gage, T. W. McDaniel, W. A. Challener, R. E. Rottmayer, G. Ju, Y.-T. Hsia, and M. F. Erden, Heat assisted magnetic recording, Proc. IEEE **96**, 1810 (2008).

[46] W. Zhang, L. Huang, C. Santschi, and O. J. F. Martin, Trapping and sensing 10 nm metal nanoparticles using plasmonic dipole antennas, Nano Lett. **10**, 1006 (2010).

[47] M. L. Juan, M. Righini, and R. Quidant, Plasmon nano-optical tweezers, Nat. Photonics **5**, 349 (2011).

[48] Y. Zhang, C. Min, X. Dou, X. Wang, H. P. Urbach, M. G. Somekh, and X. Yuan, Plasmonic tweezers: For nanoscale optical trapping and beyond, Light Sci. Appl. **10**, 59 (2021).

[49] J. Yan, P. Liu, Z. Lin, H. Wang, H. Chen, C. Wang, and G. Yang, Magnetically induced forward scattering at visible wavelengths in silicon nanosphere oligomers, Nat. Commun. **6**, 7042 (2015).

[50] B. Hopkins, D. S. Filonov, A. E. Miroshnichenko, F. Monticone, A. Alù, and Y. S. Kivshar, Interplay of magnetic responses in all-dielectric oligomers to realize magnetic fano resonances, ACS Photonics **2**, 724 (2015).

[51] Y. Zhang, P. Yue, J.-Y. Liu, W. Geng, Y.-T. Bai, and S.-D. Liu, Ideal magnetic dipole resonances with metal-dielectric-metal hybridized nanodisks, Opt. Express **27**, 16143 (2019).

[52] D. Ray, A. Kiselev, and O. J. F. Martin, Multipolar scattering analysis of hybrid metal-dielectric nanostructures, Opt. Express **29**, 24056 (2021).

[53] A. Mirzaei and A. E. Miroshnichenko, Electric and magnetic hotspots in dielectric nanowire dimers, Nanoscale **7**, 5963 (2015).

[54] S. I. Lepeshov, A. E. Krasnok, P. A. Belov, and A. E. Miroshnichenko, Hybrid nanophotonics, Phys.-Usp. **61**, 1035 (2018).

[55] E. Calandrini, A. Cerea, F. D. Angelis, R. P. Zaccaria, and A. Toma, Magnetic hot-spot generation at optical frequencies:

From plasmonic metamolecules to all-dielectric nanoclusters, Nanophotonics **8**, 45 (2019).
[56] D. Ray, T. V. Raziman, C. Santschi, D. Etezadi, H. Altug, and O. J. F. Martin, Hybrid metal-dielectric metasurfaces for refractive index sensing, Nano Lett. **20**, 8752 (2020).
[57] A. Barreda, S. Hell, M. Weissflog, A. Minovich, T. Pertsch, and I. Staude, Metal, dielectric and hybrid nanoantennas for enhancing the emission of single quantum dots: A comparative study, J. Quant. Spectrosc. Radiat. Transfer **276**, 107900 (2021).
[58] J. Hu, W. Bai, C. Tan, Y. Li, Q. Lin, and L. Wang, Highly electric field enhancement induced by anapole modes coupling in the hybrid dielectric–metal nanoantenna, Opt. Commun. **511**, 127987 (2022).
[59] A. E. Miroshnichenko and Y. S. Kivshar, Fano resonances in all-dielectric oligomers, Nano Lett. **12**, 6459 (2012).
[60] S. Lepeshov, A. Krasnok, I. Mukhin, D. Zuev, A. Gudovskikh, V. Milichko, P. Belov, and A. Miroshnichenko, Fine-tuning of the magnetic fano resonance in hybrid oligomers via fs-laser-induced reshaping, ACS Photonics **4**, 536 (2017).
[61] A. Devilez, B. Stout, and N. Bonod, Compact metallo-dielectric optical antenna for ultra directional and enhanced radiative emission, ACS Nano **4**, 3390 (2010).
[62] A. I. Barreda, H. Saleh, A. Litman, F. González, J.-M. Geffrin, and F. Moreno, Electromagnetic polarization-controlled perfect switching effect with high-refractive-index dimers and the beam-splitter configuration, Nat. Commun. **8**, 13910 (2017).
[63] T. Shibanuma, T. Matsui, T. Roschuk, J. Wojcik, P. Mascher, P. Albella, and S. A. Maier, Experimental demonstration of tunable directional scattering of visible light from all-dielectric asymmetric dimers, ACS Photonics **4**, 489 (2017).
[64] T. Feng, S. Yang, N. Lai, W. Chen, D. Pan, W. Zhang, A. A. Potapov, Z. Liang, and Y. Xu, Manipulating light scattering by nanoparticles with magnetoelectric coupling, Phys. Rev. B **102**, 205428 (2020).
[65] S. Sun, D. Wang, Z. Feng, and W. Tan, Highly efficient unidirectional forward scattering induced by resonant interference in a metal–dielectric heterodimer, Nanoscale **12**, 22289 (2020).
[66] A. Kiselev, D. Ray, and O. J. F. Martin, Multipolar scattering analysis of a hybrid metal-dielectric stacked nanoantenna, in *Plasmonics: Design, Materials, Fabrication, Characterization, and Applications XIX*, Vol. 11797, edited by D. P. Tsai, T. Tanaka, and Y.-J. Lu, International Society for Optics and Photonics (SPIE, Bellingham, WA, 2021), pp. 1–6.
[67] J. van de Groep, T. Coenen, S. A. Mann, and A. Polman, Direct imaging of hybridized eigenmodes in coupled silicon nanoparticles, Optica **3**, 93 (2016).
[68] A. E. Miroshnichenko, B. Luk'yanchuk, S. A. Maier, and Y. S. Kivshar, Optically induced interaction of magnetic moments in hybrid metamaterials, ACS Nano **6**, 837 (2012).
[69] G. Guo, T. Feng, and Y. Xu, Tunable optical pulling force mediated by resonant electromagnetic coupling, Opt. Lett. **43**, 4961 (2018).
[70] X. Fang, M. L. Tseng, D. P. Tsai, and N. I. Zheludev, Coherent Excitation-Selective Spectroscopy of Multipole Resonances, Phys. Rev. Appl. **5**, 014010 (2016).
[71] J. Zhang, K. F. MacDonald, and N. I. Zheludev, Controlling light-with-light without nonlinearity, Light Sci. Appl. **1**, e18 (2012).
[72] X. Fang, K. F. MacDonald, E. Plum, and N. I. Zheludev, Coherent control of light-matter interactions in polarization standing waves, Sci. Rep. **6**, 31141 (2016).
[73] J.-H. Yang, M.-W. Yu, and K.-P. Chen, Absorption avoided resonance crossing of hybridization of silicon nanoparticles and gold nanoantennas, Sci. Rep. **9**, 11778 (2019).
[74] C. F. Bohren and D. R. Huffman, *Absorption and Scattering of Light by Small Particles* (John Wiley & Sons, New York, 2008).
[75] J. R. DeVore, Refractive indices of rutile and sphalerite, J. Opt. Soc. Am. **41**, 416 (1951).
[76] P. B. Johnson and R. W. Christy, Optical constants of the noble metals, Phys. Rev. B **6**, 4370 (1972).
[77] B. T. Draine and P. J. Flatau, Discrete-dipole approximation for scattering calculations, J. Opt. Soc. Am. A **11**, 1491 (1994).
[78] P. C. Chaumet and A. Rahmani, Coupled-dipole method for magnetic and negative-refraction materials, J. Quant. Spectrosc. Radiat. Transfer **110**, 22 (2009).
[79] A. B. Evlyukhin, C. Reinhardt, A. Seidel, B. S. Luk'yanchuk, and B. N. Chichkov, Optical response features of si-nanoparticle arrays, Phys. Rev. B **82**, 045404 (2010).
[80] A. M. Kern and O. J. F. Martin, Surface integral formulation for 3d simulations of plasmonic and high permittivity nanostructures, J. Opt. Soc. Am. A **26**, 732 (2009).
[81] T. V. Raziman, W. R. C. Somerville, O. J. F. Martin, and E. C. L. Ru, Accuracy of surface integral equation matrix elements in plasmonic calculations, J. Opt. Soc. Am. B **32**, 485 (2015).
[82] D. Tzarouchis and A. Sihvola, Light scattering by a dielectric sphere: Perspectives on the mie resonances, Appl. Sci. **8**, 184 (2018).
[83] T. Hinamoto, M. Hamada, H. Sugimoto, and M. Fujii, Angle-, polarization-, and wavelength-resolved light scattering of single mie resonators using fourier-plane spectroscopy, Adv. Opt. Mater. **9**, 2002192 (2021).
[84] K. M. McPeak, S. V. Jayanti, S. J. P. Kress, S. Meyer, S. Iotti, A. Rossinelli, and D. J. Norris, Plasmonic films can easily be better: Rules and recipes, ACS Photonics **2**, 326 (2015).
[85] W. S. M. Werner, K. Glantschnig, and C. Ambrosch-Draxl, Optical constants and inelastic electron-scattering data for 17 elemental metals, J. Phys. Chem. Ref. Data **38**, 1013 (2009).